VIBRATION-BASED DAMAGE IDENTIFICATION OF REINFORCED CONCRETE ARCH BRIDGES USING KALMAN–ARMA–GARCH MODEL

Shuchang Zhou,* Yan Jiang,** Xiaoqing Li,*** and Qingliang Wu**

Abstract

To ensure safe operations of bridges, it is necessary to carry out the structural damage identification and safety assessment. To this end, this paper proposes a novel damage identification method based on structural health monitoring data, which is the combination of Kalman filter, autoregressive moving average (ARMA) model and generalized autoregressive conditional heteroskedasticity (GARCH) model. Firstly, the correlation between the system characteristics and the time series model is verified through the theoretical derivation of the system vibration equation. Secondly, Kalman filtering is used to preprocess the acceleration data and reduce the noise disturbance, by which a linear recursive ARMA model can be established to identify the structural damage. Then, a nonlinear recursive GARCH model is introduced to further improve the identification accuracy. Finally, the effectiveness of the proposed method is verified using the time history data obtained from the accelerated corrosion damage dynamic test of the reinforced concrete arch. The results show that: (1) the system vibrations are correlated with the time series model, whose residual variance ratio is demonstrated to be effective in identifying structural damage; (2) in the state of loading damage and corrosion damage, the identification accuracies of Kalman–ARMA are 32.8% and 75.8%, while those of the proposed method can reach 89.1% and 85.5%, respectively and (3) GARCH model can explain the heteroskedasticity hidden in the monitoring data, thereby further improving the accuracy of damage identification. Therefore, the proposed method may provide an innovative measure to assess the bridge structural condition in practice.

Key Words

Arch bridge structure, damage identification, time series, heteroskedasticity

* College of Electronic Information Engineering, Southwest University, Chongqing, 400715, China; e-mail: zsc2473823148@163.com

** College of Engineering and Technology, Southwest University, Chongqing, 400715, China; e-mail: xnjtjiangyan@163.com, wuqingliang@swu.edu.cn

*** Huashe Design Group Co., Ltd., 210014, China; e-mail: lixq@mails.cqjtu.edu.cn

Corresponding author: Yan Jiang

Recommended by Dr. Jingzhou Xin
(DOI: 10.2316/J.2021.206-0705)

1. Introduction

Due to the large structural rigidity and aesthetic appearance, arch bridges have been widely used in the traffic system, especially in mountainous areas of China. Under the coupling effects of the external complex environment and internal material degradation, the in-service arch bridges inevitably confront the risk of performance degradation [**?**], [**?**]. Therefore, the identification of the damage state of in-service arch bridges poses a critical role to master their operational status, which can facilitate structural safety and decrease post-maintenance costs.

In general, structural damage causes the variations of the physical parameters and dynamic properties, which could be captured by dynamic tests or long-term health monitoring of the structure. In recent years, many endeavours on the dynamic characteristics-based structural damage identification have been carried out [**?**], [**?**]. Based on the structural vibration information, these methods (*i.e.*, frequency-domain methods and time-domain methods) can effectively identify the damage localization and perform the subsequent quantitative analysis. Among them, the frequency-domain approaches are employed extensively because they merely take the modal parameters of the system as damage-sensitive features. For example, Calio *et al.* [**?**] discussed the eigenvalues and finite element simplification problems of the damaged spatial arch structure, and numerical simulations were carried out to explore the influences of damage simplification models on the natural frequency. In addition, some scholars had proposed structural damage identification methods for arch bridges based on modal metrics and data fusion, which could achieve better results [**?**]–[**?**]. Nie *et al.* [**?**] proposed a damage detection method based on response reconstruction phase space and carried out numerical simulation and experimental research on damage detection of circular arch structures. Tan [**?**] carried out a comprehensive probabilistic analysis on the damage identification of the main span arch rib and devised a reliable method based on dynamic fingerprint for structural damage identification. In general, the physical meaning of frequency-domain methods is clear. However,

these damage identification techniques exist in some limitations, that is, it is hard to obtain higher-order modes of large structures, complete modal vibration measurements and the optimal measurement points [**?**].

In actual application, it is easier to acquire the time-domain responses in comparison with modal parameters, and thus, the damage identification based on time-domain responses may be more convenient and effective. By contrast, this method can directly use the response data and occupy high operability. Gul *et al.* [**?**] employed the improved time series analysis method to detect and locate structural changes. However, this method was failure to achieve direct quantitative identification of damage. Du *et al.* [**?**] used the simulation data of simple-supported beam to establish an autoregressive (AR) model, which not only determined whether the structure was damaged but also identified the damage location. Obviously, the damage identification based on the linear time series models is becoming more and more mature. However, the influence of various factors, such as the internal structure and the external environment, usually can cause the structural behaviour to present some nonlinear features. In this context, the linear time series model was difficult to adapt to the need for higher precision damage identification. On this basis, a series of hybrid methods are developed to address the different data characteristics embedded in the structural behaviour. For example, Pham *et al.* [**?**] proposed a hybrid method based on the linear autoregressive moving average (ARMA) model and the nonlinear generalized autoregressive conditional heteroskedasticity (GARCH) model to explain the wear and failure of the machine. This model successfully diagnosed and predicted the future state of the machine. Chen *et al.* [**?**] applied the ARMA–GARCH model to the damage identification of three-storey building structure provided by Los Alamos National Laboratory, where a one-step ahead error prediction model was used to effectively identify the damage degree of the structure. Compared with the relatively mature linear model, the GARCH model has been less studied in the field of bridge structural damage identification and may deserve further research.

Due to the difficulty of structural damage identification as well as the insufficiency of the existing method, a new federated structural damage identification method is established by integrating Kalman filter, ARMA and GARCH models and can effectively explain both linear and nonlinear characteristics hidden in the structural behaviour. Its effectiveness is demonstrated in terms of both theoretical and applied levels.

2. Methodology

2.1 Theoretical Correlation Between System Characteristics and Time Series Models

To discover the inherent relationship between structural vibration characteristics and time series model, the following derivation is made in this paper.

Assume that a momentary force $f(t)$ acts on an object of mass m. The force analysis is shown in Fig. **??**.

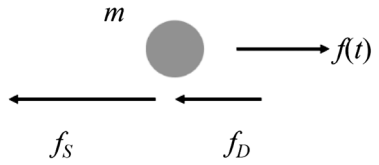

Figure 1. The force analysis of mass m.

Under the action of instantaneous force, the displacement, velocity and acceleration of mass m along the direction of instantaneous force are x, x' and x'', respectively.

The mass point m is subjected to instantaneous force $f(t)$, elastic force f_S and damping force f_D. The damping force f_D is the effect of causing structural energy loss and gradually decreasing the structural amplitude under the action of the surrounding environment and its own friction during the structural motion. Its size can be expressed as the product of the structural damping coefficient c and the particle velocity x', so the calculation expression is $f_D = cx'$. In the linear elastic structure, the elastic force f_S is linear with the deformation x, so the calculation expression is $f_S = kx$, where k is the lateral stiffness of the system. Resistance is a function that prevents physical movement, so the direction of the elastic force and the damping force is opposite to the direction of the instantaneous force.

Then, it can be calculated based on Newton's second law:

$$f(t) - f_I - f_D = mx'' \Rightarrow mx'' + cx' + kx = f(t) \quad (1)$$

The above equation is the equation of motion for a single-degree-of-freedom system. When the structure is moving, the dynamic response is related to time t. Time t can be discretized to $t = k\Delta t$, $k = 1, 2, \cdots$, then, $x(t) = x(k\Delta t) = x_k$, $f(t) = f(k\Delta t) = f_k$, where Δt is the time step and is the time interval when the data are collected. According to the definition of differentiation in higher mathematics:

$$\begin{cases} x'(t) = \frac{x_k - x_{k-1}}{\Delta t} = x'_k \\ x''(t) = \frac{x'_k - x'_{k-1}}{\Delta t} = \frac{x_k - 2x_{k-1} + x_{k-2}}{\Delta t^2} \end{cases} \quad (2)$$

Substituting (1) into (2) yields:

$$x_k - \rho_1 x_{k-1} + \rho_2 x_{k-2} = \rho_3 f_k \quad (3)$$

where ρ_1, ρ_2 and ρ_3 are all constant coefficients. Both of them can be determined by (4):

$$\begin{cases} \rho_1 = \frac{(2m + c\Delta t)}{(m + c\Delta t + k(\Delta t)^2)} \\ \rho_2 = \frac{m}{m + + c\Delta t + k(\Delta t)^2} \\ \rho_3 = \frac{(\Delta t)^2}{m + + c\Delta t + k(\Delta t)^2} \end{cases} \quad (4)$$

Compared with the ARMA model, it can be found that the vibration equation of the single-degree-of-freedom system after time discretization satisfies the ARMA(2,0) distribution. The same reason can be proved that when the structure is a multi-degree-of-freedom system of n degrees

of freedom, the vibration equation of the structure can be represented as:

$$Mx'' + Cx' + Kx = f(t) \tag{5}$$

where M, C and K are the nth-order mass matrix, damping coefficient matrix and stiffness matrix in the structural system, respectively.

The n-order matrix equation is equivalent to the 2n-order non-homogeneous differential equation, which can be converted into:

$$\begin{aligned} &a_{2n}x^{(2n)} + a_{2n-1}x^{(2n-1)} + \cdots + \alpha x' + \alpha_0 x \\ &\quad = \beta_{2n-2}f^{(2n-2)} + \beta_{2n-3}f^{(2n-3)} + \cdots + \beta f' + \beta_0 f \\ &\quad \Rightarrow x_k = \sum_{i=1}^{2n} \alpha_i x_{k-i} + b_0 f_k \sum_{j=1}^{2n-2} \beta_j f_{k-j} \end{aligned} \tag{6}$$

where $\alpha_i,\ i = 1, 2\cdots, 2n,\ \beta_j,\ j = 1, 2\cdots, 2n$ are all constant coefficients, x_{k-i} is regarded as the lag response of $k-i$ order and f_{k-j} is regarded as the lag disturbance term of the $k-j$ order, that is, the vibration equation of the multi-degree-of-freedom system obeys the ARMA (2n, 2n-2) process.

It can be found that the vibration equation of the structure can be expressed as an ARMA process, whether it is a single-degree-of-freedom system or a multi-degree-of-freedom system. It shows that the modelling method of the ARMA model is based only on the system output and does not require structural input information. Therefore, this method is extremely convenient and reliable for engineering that easily acquires structural responses but is inconvenient to measure structural input information. The external excitation can be regarded as the disturbance term of the model. The structural response is different due to the different applied loads. The internal physical properties of the structure are changed dynamically in response to the applied load. In many damage identification studies, the interference signals existing in the data acquisition are regarded as Gaussian white noise, the data noise reduction processing is performed for white noise and the damage identification is analysed by analysing the statistical features of the data. Therefore, the ratio of the residual and variance of the model to those of the intact structure are used as the damage sensitive characteristic feature (DSF) in this paper, and this index can be used to characterize the state of the structure, by which the structural damage can be identified directly using the time-series signal. The formula is as follows:

$$DSF = \frac{\sigma^2(\varepsilon_d)}{\sigma^2(\varepsilon_u)} \tag{7}$$

where DSF is the damage index, and $\sigma^2(\varepsilon_d)$ and $\sigma^2(\varepsilon_u)$ are the variance of the residual sequence generated by damage structure and lossless structure, respectively.

2.2 Kalman Filter Algorithm

Due to the complex monitoring environment of the bridge structures, there may be a large amount of random noise in the monitoring data [**?**]. To this end, this paper uses the optimal estimation Kalman filter algorithm in the sense of minimum mean square error to perform random noise reduction on the data. In most cases, the main application is the discrete Kalman filter [**?**], [**?**], and its mathematical model, including the state equation and the observation equation, is as follows:

$$X_k = -F_{k|k-1}X_{k-1} + G_{k|k-1}W_{k-1} \tag{8}$$

$$Z_k = H_k X_k + V_k \tag{9}$$

where X_k is the state vector of the system at time k, and X_k is evolved from the state at time $(k-1)$ according to (8). $F_{k|k-1}$ is the state transition matrix from time $(k-1)$ to time k, and $F_{k|k-1}$ is applied to the previous state X_{k-1}. $G_{k|k-1}$ is the noise input matrix from time $(k-1)$ to time k. W_k is the process noise (or system noise) which is assumed to be drawn from a zero mean multivariate normal distribution, that is, $W_k \sim N(0, Q_k)$, where Q_k is the covariance of the process noise. Z_k is the observation matrix (or measurement matrix) of the true state X_k at time k. H_k is the observation matrix which maps the true state space into the observed space, V_k is the observation noise (or measurement noise) which is assumed to be zero mean Gaussian white noise, that is, $V_k \sim N(0, R_k)$, where R_k is the covariance of the observation noise. W_k and V_k are all assumed to be mutually independent.

2.3 Autoregressive Moving Average Model

Given a time series of data X_t, the ARMA model is a tool for understanding and, perhaps, predicting future values in this series. The AR part involves regressing the variable on its own lagged (*i.e.*, past) values. The moving average (MA) part involves modelling the error term as a linear combination of error terms occurring contemporaneously and at various times in the past. The model is usually referred to as the ARMA(p, q) model, where p is the order of the autoregressive polynomial (AR part) and q is the order of the moving average polynomial (MA part).

Thus, ARMA(p, q) can be defined as:

$$X_t = c + \varepsilon_t + \sum_{i=1}^{p} \varphi_i X_{t-i} + \sum_{i=1}^{q} \theta_i \varepsilon_{t-i} \tag{10}$$

where c is a constant, ε_t, ε_{t-1}, ... are disturbance terms (white noise error terms), $\varphi_1, \ldots, \varphi_p$ are the AR model's parameters and $\theta_1, \ldots, \theta_q$ are the MA model's parameters.

2.4 GARCH Model

Under the premise that the variance of the disturbance term is constant, the ARMA model can better reflect the linear time series process. However, due to the interference of external environments such as temperature and noise, the ARMA model has poor stability of disturbance variance. It will change with time and is related to the variance of the past time [**?**]. The continued use of AR models under conditions that are inconsistent with the assumptions will inevitably lead to a reduction in the accuracy of the time series models [**?**]. Therefore, Engle *et al.* [**?**] devised an ARCH model to characterize the variation of the variance

of the perturbation term sequence over time. The main idea of the ARCH model is that the conditional variance σ_t^2 of u_t at time t depends on the residual square u_{t-i}^2 of the time $(t-i)$. The ARCH(p) expression is as follows:

$$\sigma_t^2 = \alpha_0 + \sum_{i=1}^{p} \alpha_i u_{t-i}^2 \tag{11}$$

It can be known from (11) that the conditional variance consists of a number of residual squared weighted sums, that is, the ARCH model is a distributed lag model of σ_t^2. Therefore, Bollerslev [**?**] proposed the GARCH model, replacing a large number of hysteresis values u_t^2 with a very small number of hysteresis values σ_t^2, thereby greatly reducing the number of parameters and improving the accuracy of parameter estimation. In the GARCH model, there are two different settings need to be considered, including the conditional mean and the conditional variance. The GARCH(q,p) conditional variance can be expressed as:

$$\sigma_t^2 = \omega + \sum_{j=1}^{q} \beta_j \sigma_{t-j}^2 + \sum_{i=1}^{p} \alpha_i \sigma_{t-i}^2 \tag{12}$$

where ω is a constant term, p and α_i are the order and coefficient of the MA ARCH term, respectively. q and β_i are the order and coefficient of the AR GARCH term.

2.5 Proposed Method

2.5.1 The Framework of the Proposed Method

In this paper, the damage identification of the arch is carried out by the combination of Kalman filtering, ARMA and GARCH models. The workflow of the proposed method is presented in Fig. **??** and the details are listed below:

1. The Kalman filter is used to effectively reject the random noise and noise-reduced is applied to the test acceleration data.
2. The AR model is ordered and its parameters are determined to pass the ARCH term test.
3. The nonlinear recursive GARCH model is introduced to take into account the heteroskedasticity and other problems of the linear time series model.
4. The damage-sensitive feature index is used to identify the damage to the structure.

In summary, the combination of the three methods overcomes the problems of random errors accompanying the experimental data and the lack of heteroskedasticity of the linear time series model to effectively improve the accuracy of the method for structural damage identification.

3. Experiment

3.1 Details of Test Model

A total of two equal-section reinforced concrete arches were made for the model test, 0# arch was corrosion-free arch and 1# arch was a corrosion arch. Longitudinal

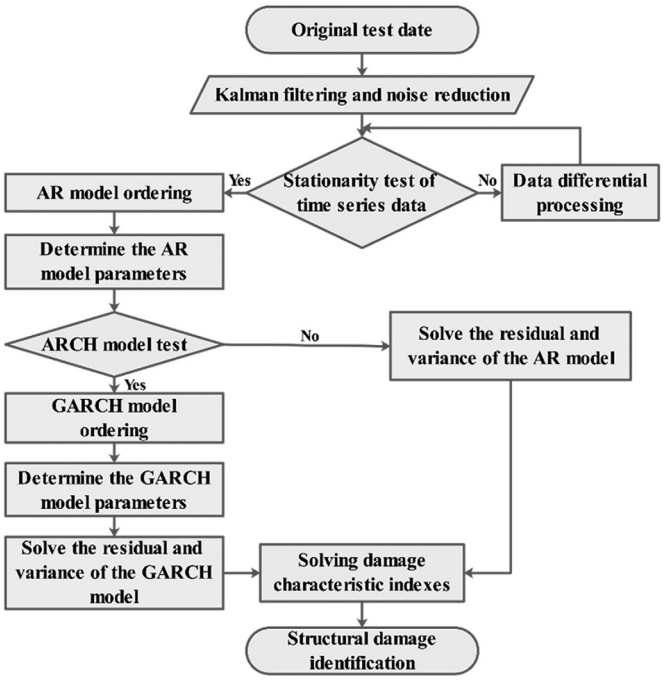

Figure 2. Flow chart of damage identification algorithm.

reinforcement was 12 mm HRB400 steel bar, stirrup was 6 mm HRB235 steel bar and the stirrup spacing was taken as 100 mm; the distance from the centre of the longitudinal reinforcement to the edge of the concrete section was 25 mm. Through testing, the compressive strength of the concrete shaft of 0# and 1# arch rib was 33.08 and 30.21 MPa, respectively. The test arch geometry parameters are shown in Table **??**.

3.2 Formation of the Damage

To accurately simulate the decay characteristics of the corrosion damage characteristics of the actual structure, the accelerated simulation scheme of the galvanic current corrosion of the outer sponge after the first weight loading was adopted in this paper.

The test arch steel bar and the stainless steel mesh are respectively used as the positive electrode and the cathode to completely wrap each segment. Then the stainless steel mesh was wrapped with a water-retaining sponge moistened with 5% NaCl solution, and the silicone tube with an inner diameter of 5 mm was used in combination with the flow rate regulator. The 5% NaCl solution was continuously transported to the corrosioned section and wrapped with a water-retaining film to reduce water evaporation and the water loss, so as to ensure that the water-retaining sponge maintains long-term humidity where the power was accelerated and corrosioned. The weight design of the dead load and accelerated corrosion of the test arch is shown in Fig. **??**.

3.3 Acquisition of Acceleration Data

In this paper, acceleration time data acquisition is carried out with the DH5922N Donghua Dynamic Signal Acqui-

Table 1
Basic Parameters of Test Arch

Net Span	Net Height	Vector Span Ratio	Section Size	Wide Span Ratio	Sectional Form	Arch Axis Coefficient	Reinforcement Ratio
4.2 m	0.84 m	1/5	$b \times h = 0.24$ m $\times$ 0.12 m	1/17.5	Solid section	1.67	2.35%

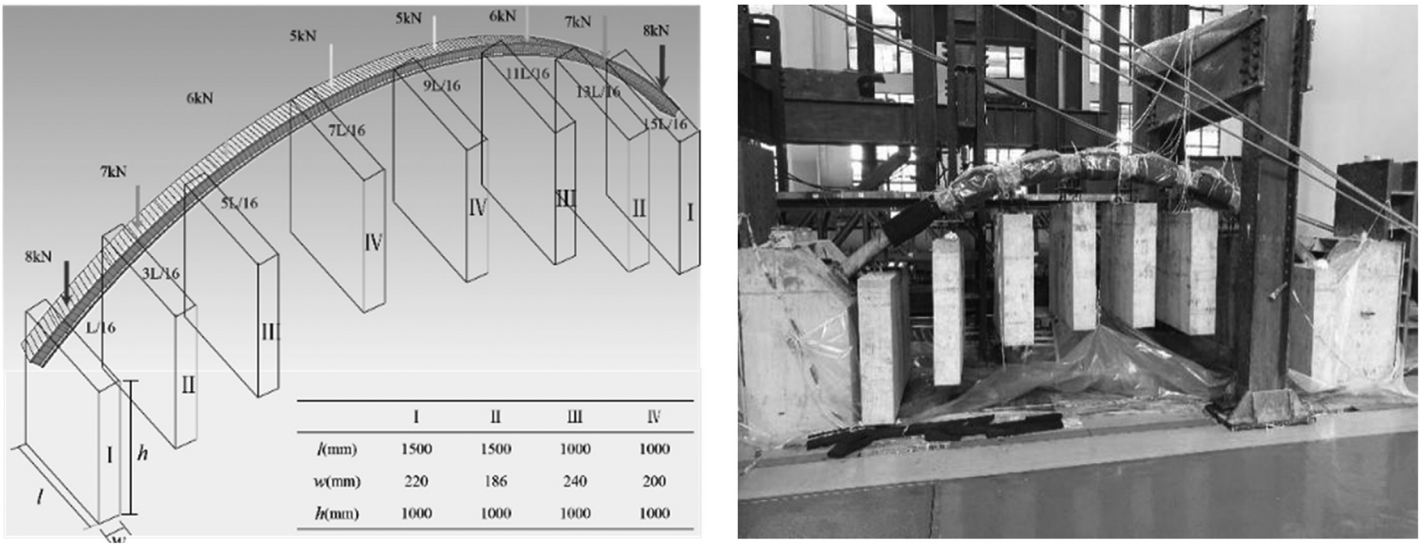

(a) (b)

Figure 3. Accelerated corrosion scheme under weight load: (a) the weight design of the dead load and (b) accelerated corrosion test site.

sition and Analysis System and devices such as dynamic signal collectors and acceleration sensors.

To accurately obtain the vertical acceleration of the structure, the steel plate pedestals were made according to the arch back at different positions before the test and glued to the centre of the specified sections. Acceleration sensors were placed on those sections and hammered to obtain the structural dynamic time history data. And the collecting instrument was directly connected to the earth to reduce the interference of the electromagnetic signal. The hammer was free to fall 15 cm above the excitation position to ensure the same excitation force. The accelerometers and the displacement meters were arranged in the middle of each weight block and were recorded as channel 1–channel 7; the specific measurement points are shown in Fig. **??**.

When the power test was completed, the concrete of the test arch was chiselled, the reinforcement was removed and its mass loss rate was measured after being rinsed with water $\rightarrow$ soaked in oxalic acid solution $\rightarrow$ cleaned with water $\rightarrow$ dried. After the test, the corrosioning rate of the whole arch at different locations was less different, and the average corrosioning rate of the whole arch was 6.85%.

4. Application of the Proposed Method

4.1 Building of the Time Series Model

In this paper, the dynamic tests of two model arches were carried out, which were recorded as 0# arch and 1# arch, respectively, where 0# arch was the intact arch rib and 1# arch was the accelerated corrosion damage arch rib. In the experiment, the loading method used four-point single-point loading, loading to single hinge formation. For the 0# arch model, the dynamic time history response data before loading were recorded as $\{A_t\}$ and the time history data after loading damage were recorded as $\{B_t\}$. The time history data after 1# corrosion arch model were recorded as $\{C_t\}$, that is, $\{A_t\}$ represented a good benchmark, $\{B_t\}$ represented the loading damage state and $\{C_t\}$ represented the corrosion damage state. Since the 1# arch rib needed electrochemical corrosion, it was inconvenient to install the steel backing plate for time history data acquisition before the corrosion. Considering that the arch rib model was similar, the simultaneous pouring and the arch rib installation position were fixed in the same positon; the 0# arch reference state was taken as 1# arch reference state for comparative analysis. The test results were used to define the loading damage index and the corrosion damage index. The time series model was established based on time history data, and the residual variance ratio was constructed as the damage index.

The qualitative damage identification study and quantitative damage analysis were carried out by analysing quantitative damage indicators and the interrelationship between damage characteristics factors in different states, and working conditions were divided as shown in Fig. **??**.

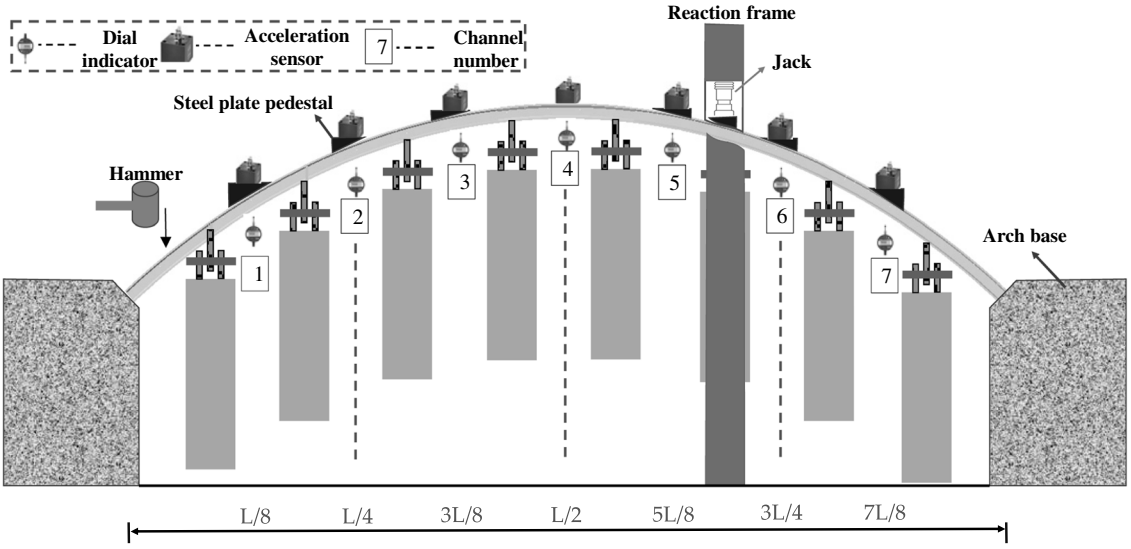

Figure 4. Power data collection.

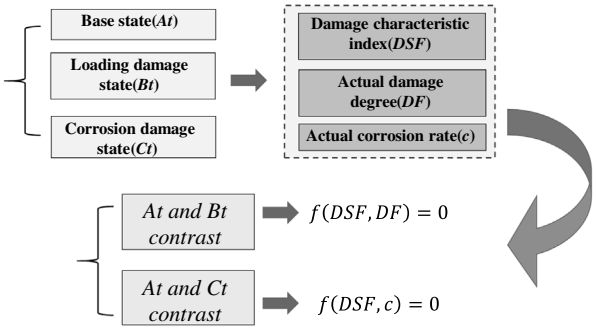

Figure 5. Damage identification diagram.

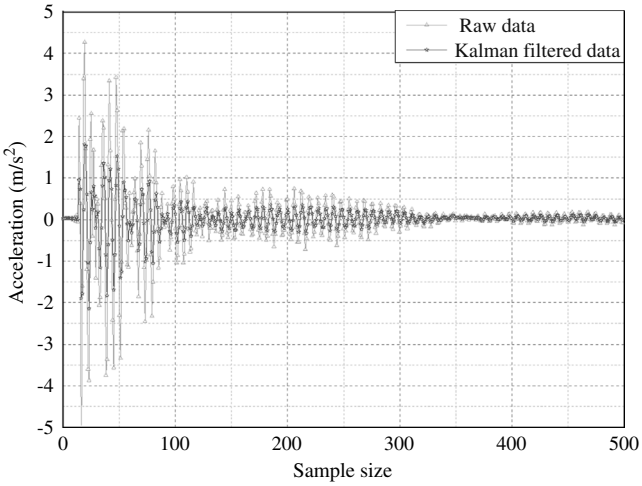

Figure 6. Kalman filtered data.

4.1.1 Noise Reduction of Acceleration Data

During the experiment, due to the large influence of random errors such as light, temperature and instrument, the Kalman filter is used to reduce the noise of the raw data. Existing studies indicate that there is a positive correlation between the measured noise variance and the estimated performance of the filter, and the system noise variance has a negative correlation with the filter performance of the filter [**?**]. After several times of optimization, the original data of the test showed that when relevant parameters, R_k and Q_k, were met $R_k = 2.0$ and $Q_k = 0.5$, the noise reduction effect was better. The time series processed by Kalman filter was recorded as $\{a_t\}$. As shown in Fig. **??**, Kalman filter method can effectively reject random noise and the fidelity of the filtered data is better.

4.1.2 Building of the Autoregressive Moving Average Model

The following data analysis takes the acceleration time response data of arch 0# intact condition as an example and describes the time series model analysis process and specific steps in detail.

(1) Data stationarity test

The augmented Dichey–Fuller test was used to develop the data smoothness test [**?**]. The summary of smoothness test parameters for each channel of arch 0# is shown in Table **??**. The t-statistic is the critical value of the parameter estimate, and the P-value indicates the probability value of rejection of the original hypothesis. When $P <$ a, then the series test can be considered as rejecting the original hypothesis, that is, admitting that there is no unit root in the series and the series satisfies the smoothness requirement, where α is the significance level, which is taken as 0.05 in this paper.

(2) Model identification

The Box–Jenkins model identification method is used in this paper to obtain the appropriate time series model process. The autocorrelation and partial autocorrelation features reflected by the sample data are employed to determine the optimal linear time series model.

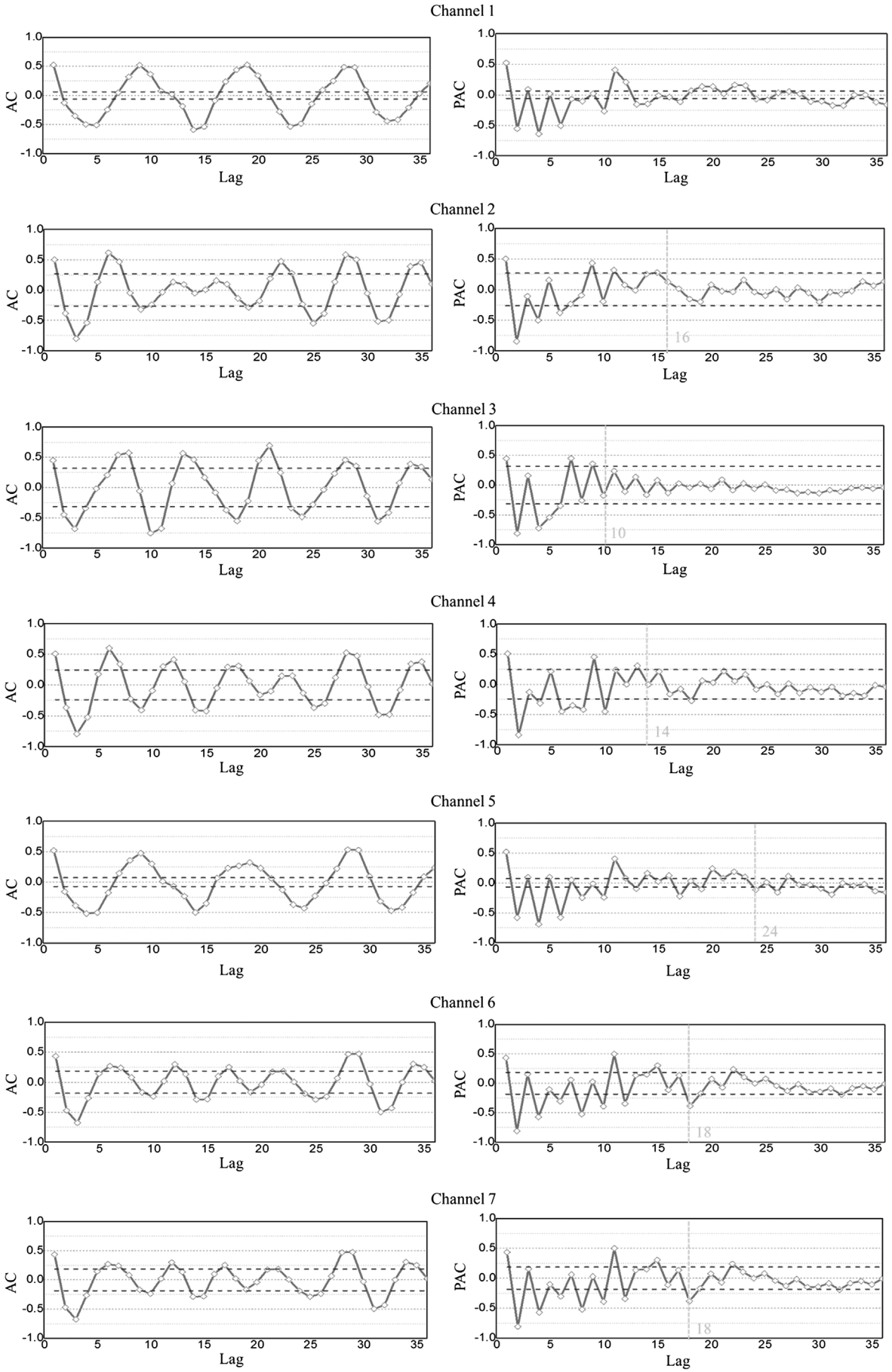

Figure 7. The time history data correlation diagram of 0# arch before loading.

Table 2
Stationarity Test Parameter

	Channel 1	Channel 2	Channel 3	Channel 4	Channel 5	Channel 6	Channel 7
Statistics t	−8.160	−7.266	−3.173	−6.144	−8.349	−5.763	−6.820
1% Confidence interval threshold	−3.44369	−3.44358	−3.44369	−3.44358	−3.44369	−3.44366	−3.44369
Value p	0.000	0.000	0.022	0.000	0.000	0.000	0.000
Hypothesis	H_1	H_1	H_1	H_1	H_1	H_1	H_1

According to the correlation of the time history data before 0# arch loading, the autocorrelation function (ACF) and partial autocorrelation function (PACF) of each channel can be obtained as shown in Fig. **??**. As seen in the figure, the PACF of each channel shows oscillatory ups and downs, and the values of each order function are outside the standard value (2 times the standard deviation range) and are not obviously truncated, so the model is judged to be incompatible with the MA process. From the plot of the PACF) for each channel, it can be found that the values of the first few orders of the model are clearly outside the standard values. However, as indicated by the yellow line in the figure after the P-order, the PACF values of channels 1–7 all fall significantly within the 95% confidence interval, where the function values of channels 1 and 5 fluctuate slightly within the standard values, but both are very small compared to the standard values and can be approximated as presenting function values falling within the 95% confidence interval outside the P-order. Further data analysis of channels 1 and 6 sequences revealed that the value of PACF for channel 1 met the 95% confidence interval when $P = 32$. Similarly, the value of the PACF for channel 5 needs to be satisfied after 34th order, both indicating that the time-course data exhibit a distinct AR process.

Therefore, the AR model should be chosen to model the time-course data before 0# arch loading more significantly and effectively. It can be understood that the AR model order can be initially determined after the PACF plot, and when P is taken as 10∼34, the time-course data of each channel satisfy the AR model.

(3) Model Order

In this paper, the Akaike information criterion (AIC) is used to determine the orders of ARMA and GARCH models, and its specific expression is given by:

$$AIC(x) = 2x + X \ln\left(\hat{\sigma}_a^2\right) \tag{13}$$

where $x = p+q$ is the number of independent parameters in the model, X is the number of sample data and $\hat{\sigma}_a^2$ stands by the maximum likelihood estimation of the residual variance.

The time history data are calculated as a summary of the model's fixed-order parameters corresponding to each channel, as shown in Fig. **??**. R^2 represents the goodness of fit of the P-order AR model. The closer the value to 1, the better the fitting result. From the figure, it can be seen that when P is small, the value of R^2, the goodness of fit of the model, is small, and as P increases, R^2 gradually increases and approaches to 1. A gradual increase in the P value will gradually reduce the AIC value, in line with the AIC guidelines described in the previous section. The change in R^2 is small when P reaches a certain order, that is, an increase in P only leads to an increase in the model parameters and does not cause a significant increase in R^2 when the goodness of fit is guaranteed to a certain value. Although the AIC value corresponding to the P-value is not taken to be the minimum value at this time, it is considered that the increase in the number of parameters significantly leads to a decrease in the accuracy of the parameter estimation. Therefore, in this paper, the goodness of fit of 0.8 is taken as the acceptable fit of the model, and the model is ordered by combining the number of model parameters. When P reaches 10, there are six channels with data $R^2 > 0.80$ and one channel with data $R^2 < 0.80$ (channel 7), and when P reaches 19, all seven channels with data $R^2 > 0.80$. Taking into account the amount of information covered by the model and fitting effect, the order of the model for time-course data is determined to be 10.

(4) Parameter estimation and applicability test

In this paper, parameter estimation is carried out for the time history data before 0# arch loading, and the results are shown in Table **??**. a_t denotes the magnitude of the acceleration at time t and the pre-constant term of a_{t-p}, φ_p, is the P-order coefficient of the AR model. The model for each channel is established as follows, and the parameters in the equation refer to Table **??**.

4.1.3 Establishment of GARCH Model

(1) ARCH Test

It can be seen from the above study that the statistics of linear time series equations are prominent and the degree of fitting is good, but considering the heteroskedasticity of the data, it is necessary to test whether the error terms of these equations have conditional heteroskedasticity. The residual squared correlation plot of the AR model is obtained according to each fitting equation (as in Fig. **??**), where ACF and PACF denote the residual squared ACF and PACF of the AR(10) model, respectively. It can be seen that both ACF and PACF exhibit certain volatility. Except for channels 3 and 7, the ACF and PACF values of the other channels show truncation characteristics, indicating that the time-course data AR model is heteroskedastic and

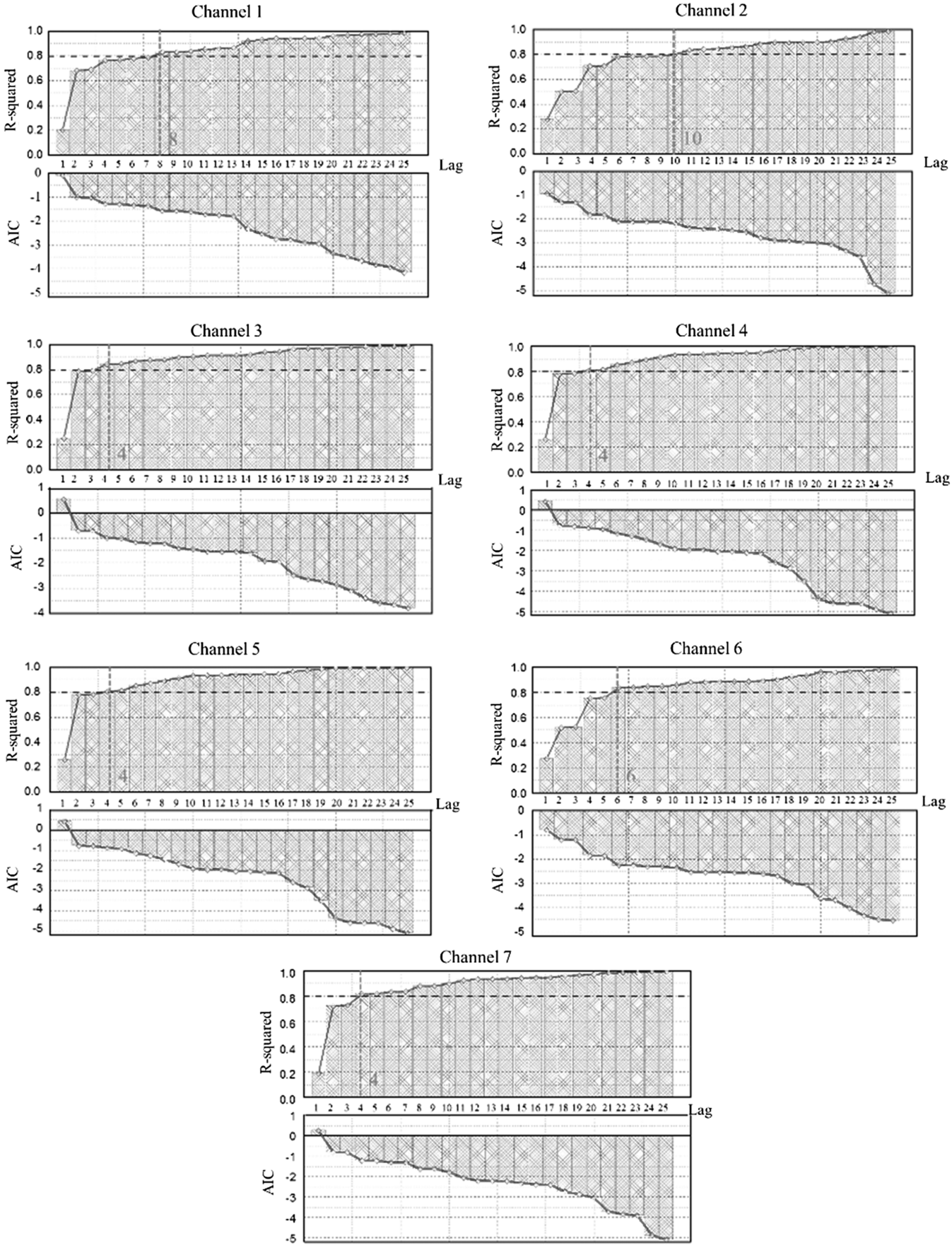

Figure 8. Data model order of 0# arch before loading.

Table 3
Summary of AR(10) Model Parameter Estimation

		c	a_{t-1}	a_{t-2}	a_{t-3}	a_{t-4}	a_{t-5}	a_{t-6}	a_{t-7}	a_{t-8}	a_{t-9}	a_{t-10}
Channel 1	Coefficient	−0.013	0.984	−1.602	0.856	−1.277	0.673	−1.182	0.658	−0.715	0.155	−0.202
	Significant Level	0.006	0.006	0	0	0	0	0	0	0	0	0.014
Channel 2	Coefficient	−0.001	−0.001	0.91	−1.424	0.985	−1.408	0.656	−0.938	0.317	−0.501	0.266
	Significant Level	0.744	0.744	0	0	0	0	0	0	0.001	0	0
Channel 3	Coefficient	−0.01	−0.01	0.927	−1.327	0.633	−1.167	0.737	−0.682	0.516	−0.682	0.596
	Significant Level	0.052	0.052	0	0	0	0	0	0	0	0	0
Channel 4	Coefficient	0	0	0.907	−1.541	0.754	−0.942	0.631	−1.073	1.159	−0.784	0.511
	Significant Level	0.966	0.966	0	0	0	0	0	0	0	0	0
Channel 5	Coefficient	0	0	1.043	−1.345	0.686	−1.471	1.074	−1.175	0.669	−1.175	0.834
	Significant Level	0.939	0.939	0	0	0	0	0	0	0	0	0
Channel 6	Coefficient	0.006	0.006	1.098	−1.884	1.598	−2.151	1.331	−1.491	0.669	−0.681	0.256
	Significant Level	0.071	0.071	0	0	0	0	0	0	0	0	0.0001
Channel 7	Coefficient	0.003	0.003	0.988	−1.975	1.16	−1.923	0.991	−1.772	0.963	−1.245	0.414
	Significant Level	0.468	0.468	0	0	0	0	0	0	0	0	0

it is more reasonable and effective to use the GARCH model to explain the program column.

(2) Model order

The ARCH term is tested using the LM (Lagrange Multiplier) statistic for each channel time-course data, and the test results are summarized in Table **??**. The LM statistics and the corresponding probabilities for each channel after 1, 5, 10 and 20 orders of lag are listed in the table. Where the P-value is the probability of rejection, and when $P < \alpha$ indicates the significance level, taken as 0.05, the original hypothesis is rejected. When $H = 0$, it indicates that the ARCH term tests the original hypothesis (a_t has homoskedasticity), and when $H = 1$, it indicates that it has a_t heteroskedasticity. It can be seen that the LM test for each channel is shown as rejection of the null hypothesis, that is, the time history data sequence is recognized to have a certain heteroskedasticity, and the nonlinear time series model should be further used for analysis. At the same time, it is noted that when the model lags 20th order, the sequence still rejects the null hypothesis, and the lag order is higher but there is still heteroskedasticity. It is considered that the data have a high-order ARCH effect, and low-order GARCH model should be used for analysis.

In summary, the time history data have a high-order ARCH effect. Considering the parameter estimation error, the GARCH(1,1) model was initially selected.

(3) Parameter estimation and applicability test

After the order of the GARCH model was determined, the model parameters were estimated by the maximum likelihood method. The results of parameter estimation for each channel before 0# arch loading are summarized in Table **??**. The final form of the model is determined by:

$$\hat{a}_t = c + \beta_1 a_{t-1} \tag{14}$$

$$\hat{a}_t^2 = k + \gamma_1 \hat{u}_{t-1}^2 + \delta_1 \hat{\sigma}_{t-1}^2 + \hat{\varepsilon}_t \tag{15}$$

where c and k are constant coefficients, β_1, γ_1 and δ_1 are the coefficients of a_{t-1}, $\hat{u}_{t-1}^2$ and $\widehat{\sigma}_{t-1}^2$, respectively; for specific values, refer to Table **??**.

It can be found in the table that except for the constant term coefficients, the rest of the coefficients do not appear to be significantly 0 or close to 0, and the parameter significance is significantly 0, indicating that the parameter estimation features are significant. Therefore, it is determined that the GARCH(1,1) model can better reflect the variation pattern of the series.

4.2 Damage Index

The AR model and the GARCH model were established using the time history data after 0# arch loading and the time history data before 1# arch loading, respectively, and the damage indexes under different damage conditions were obtained according to (7). The summary was shown in Table **??**. There were no acceleration sensors at the position of channels 5 and 6 of 1# arch due to corrosion damage, so there was no damage index. The working condition A_t also shows no loading damage and no corrosion damage state, so working condition A_t is used as the reference state. The residual variance ratios of working condition B_t and working condition A_t are the damage characteristic factors considering only the loaded damage

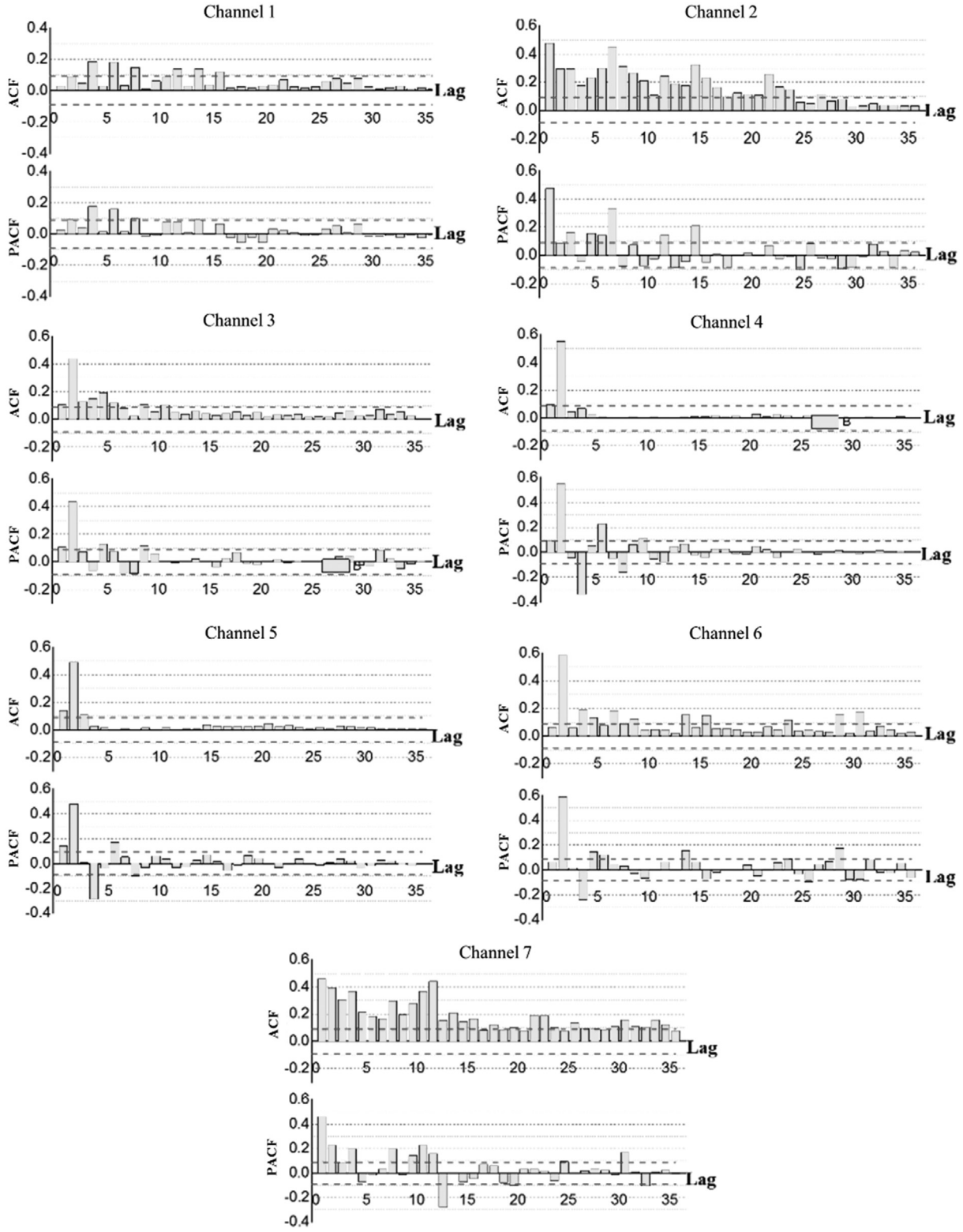

Figure 9. The residual squared correlation graph of AR model.

case. The residual variance ratio of working condition C_t and working condition A_t is the damage characteristic factor considering only the corrosion accelerated damage state.

As can be seen in the table, both the damage to be measured state after loading, the damage state after corrosion and the damage feature factor corresponding to AR model and GARCH model demonstrate significant differences under the same channel, indicating that damage feature factor can identify damage and confirm feasibility of the feature factor.

Table 4
Result of LM Statistic Test

Lag order	Channel 1			Channel 2			Channel 3			Channel 4			Channel 5			Channel 6			Channel 7		
	LM	P	H	LM	P	H	LM	P	H	LM	P	H	LM	P	H	LM	P	H	LM	P	H
1	0.3	0.564	0	110.6	0	1	5.7	0.017	1	4.3	0.038	1	9.5	0.002	1	1.9	0.169	0	103.3	0	1
5	180.7	0	1	130.9	0	1	143.7	0	1	187.7	0	1	149.4	0	1	191	0	1	140.7	0	1
10	254.2	0	1	307.8	0	1	367.3	0	1	225.5	0	1	180.6	0	1	163.7	0	1	209.3	0	1
20	291	0	1	335.1	0	1	251.3	0	1	291.9	0	1	308.3	0	1	185.7	0	1	392.2	0	1

Table 5
Summary of GARCH(1,1) Model Parameter Estimation

		Mean Equation		Variance Equation		
		c	a_{t-1}	k	$\hat{u}_{t-1}^2$	$\widehat{\sigma}_{t-1}^2$
Channel 1	Coefficient	0	0.581	0	0.038	0.951
	Significant level	0.842	0	0.458	0	0
Channel 2	Coefficient	0.001	0.8	0	0.641	0.561
	Significant level	0.208	0	0.127	0	0
Channel 3	Coefficient	0.016	0.611	0	1.677	0.275
	Significant level	0	0	0.056	0	0
Channel 4	Coefficient	−0.002	0.562	0	0.95	0.453
	Significant level	0.289	0	0.585	0	0
Channel 5	Coefficient	0.004	0.635	0	0.836	0.427
	Significant level	0.024	0	0	0	0
Channel 6	Coefficient	0.002	0.705	0	0.935	0.445
	Significant level	0	0	0.005	0	0
Channel 7	Coefficient	0.002	0.577	0	0.302	0.69
	Significant level	0.586	0	0	0	0

4.3 Actual Damage Degree

4.3.1 Loading Damage Indicator

Established studies show that the relationship between concentrated force F and span deflection w at three-dimensional level under load is shown in Fig. **??**, and that loading damage process is divided into the following three stages: crack initiation (I_a), yielding of the longitudinal tensile reinforcement (II_a) and structural damage (III_a). Correspondingly, the stress and strain evolution of the two-dimensional positive section is shown in Fig. **??**. Therefore, based on the flat section assumption, the approximation of the section curvature ϕ is calculated as follows:

$$\phi \approx \tan\phi = \frac{\varepsilon}{x} \tag{16}$$

where ϕ is the section curvature of a certain stress stage, ε is the strain of the upper edge section under the action of concentrated force and x is the height of the equivalent compression zone of the section.

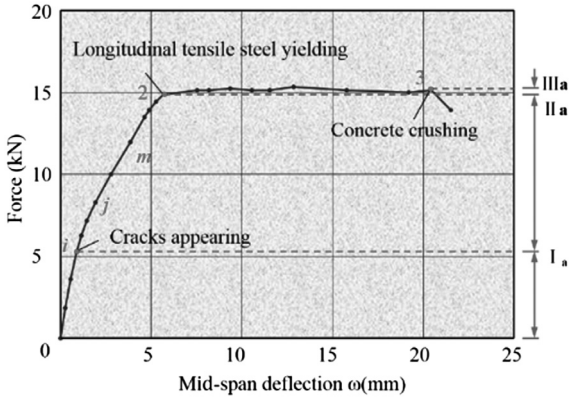

Figure 10. Typical load-deflection (F–w) curve.

Table 6
Summary of Damage Indexes Under Different Working Conditions

	(a) AR(10) Model							
	Working Condition	Channel 1	Channel 2	Channel 3	Channel 4	Channel 5	Channel 6	Channel 7
Residual variance	A_t	0.105	0.079	0.114	0.089	0.091	0.073	0.097
	B_t	0.05	0.031	0.056	0.047	0.047	0.038	0.043
	C_t	0.055	0.062	0.046	0.059	/	/	0.05
DSF	B_t/A_t	0.475	0.384	0.494	0.528	0.514	0.517	0.438
	C_t/A_t	0.524	0.78	0.398	0.657	/	/	0.51
	(b) GARCH(1,1) Model							
	Working Condition	Channel 1	Channel 2	Channel 3	Channel 4	Channel 5	Channel 6	Channel 7
Residual variance	A_t	0.232	0.158	0.319	0.359	0.302	0.166	0.278
	B_t	0.143	0.088	0.2	0.214	0.211	0.139	0.169
	C_t	0.189	0.143	0.178	0.257	/	/	0.154
DSF	B_t/A_t	0.616	0.558	0.627	0.597	0.698	0.834	0.606
	C_t/A_t	0.813	0.903	0.56	0.714	/	/	0.553

Note: The residual variance value in the table is accurate to 0.001, and the *DSF* value is the actual residual variance.

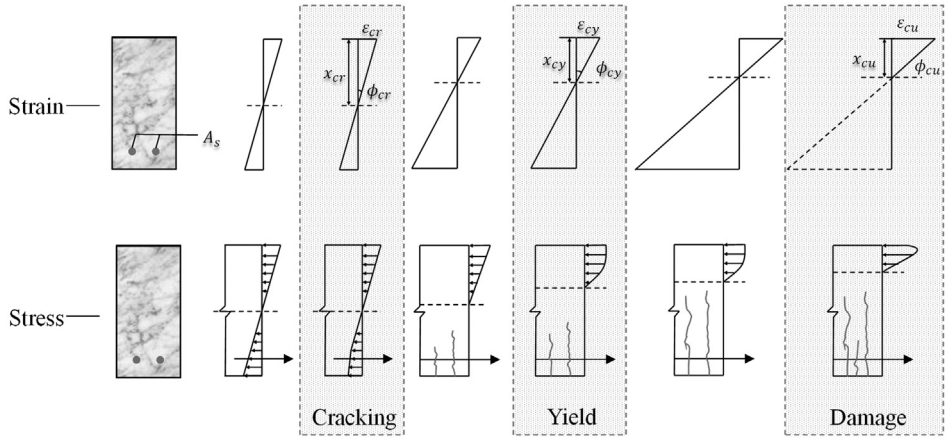

Figure 11. Strain and stress distribution at each stage.

In Fig. **??**, ε_{cr}, ε_{cy} and ε_{cu} represent the strain magnitudes of the upper edge section when the section is cracked, reinforcement is to yield and the section is broken under the action of concentrated force. x_{cr}, x_{cy}, x_{cu} and ϕ_{cr}, ϕ_{cy}, ϕ_{cu} correspond to the strain, indicating the compression height and section curvature at the corresponding stage.

A large number of tests have shown that the moment-curvature ($M-\phi$) curve is roughly composed of three straight lines, and the typical moment-curvature curve is shown in Fig. **??**. In the figure, ϕ_{cr} denotes the curvature of the cross-sectional crack, and ϕ_{cy} denotes the corresponding section curvature when the steel yields. M_{cr} denotes the bending moment of the section when the crack occurs, and M_{cy} denotes the bending moment of the section when the steel is to yield. The bending moment curvature satisfies the following formula:

$$\varphi(x) = \frac{M}{EI} \tag{17}$$

where EI is the structural bending stiffness. The two-dimensional section stiffness often uses the secant of different nodes as the stiffness under different conditions. As shown in Fig. **??**, it is often defined that the section stiffness before concrete cracking is the initial stiffness, the secant stiffness is the section cracking stiffness when cracking and the secant stiffness after cracking to the yield of the steel is the stiffness of the steel when yielding.

The comparison between Figs. **??** and **??** indicates the curves in the figure can be divided into three stages according to the corresponding cracking point, steel yield point and failure point. The slope change in the bending moment-curvature curve characterizes the change in

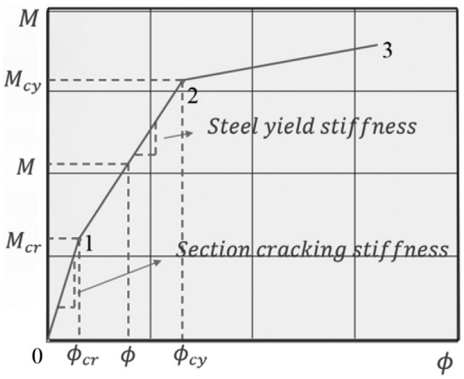

Figure 12. Moment-curvature typical curve.

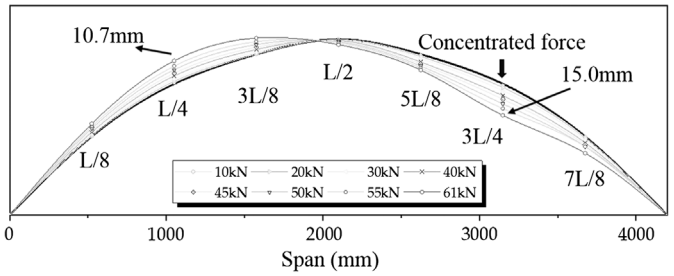

Figure 13. Overall load–displacement curve of 0# model arch.

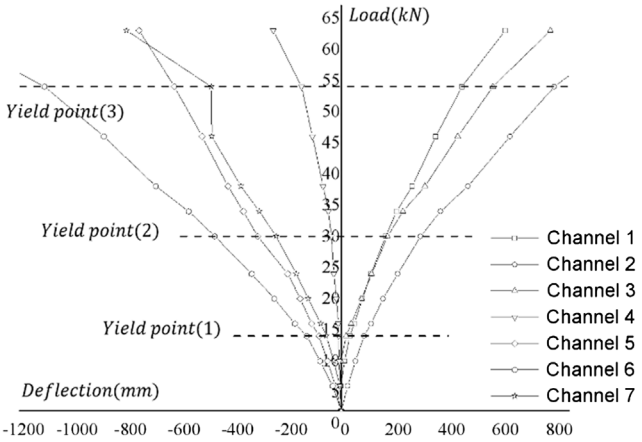

Figure 14. Load–deflection curve of each point of model arch.

cross-sectional stiffness, then the slope corresponding to different phase points in the load–displacement curve can also be considered to characterize the change in the internal properties of the structure. The difference is that the bending moment-curvature curve reflects the two-dimensional cross-sectional stiffness damage characteristics, while the load–displacement curve can be used to characterize the three-dimensional macrostructural damage characteristics. The load–displacement curve is usually used to reflect the softening characteristics of concrete materials. The softening property of concrete is the damage. The deterioration process of materials and structures is the process of damage formation and accumulation. Therefore, the load–displacement curve of three-dimensional structure is proposed in this paper.

Structural stiffness changes are often used to characterize the degree of structural damage. When the stiffness changes to a certain value, the structure is considered to have a corresponding degree of damage. Considering that the structure in the actual project is mostly with crack working state. It is more in the stage of crack occurrence and the yielding stage of steel. It is difficult to reach the stage of structural failure. When the structural load response test is performed to obtain the structural response, the load deflection curve appears as the "0–2" curve in Fig. **??**. Where point m is the damage state to be measured, segment $0i$ is the structural line elastic phase, the slope value k_{0i} of the linear elastic phase is taken as the reference value and the node j (the intermediate point of i and m) is introduced as the reference point. Define the slope change rate of each segment as the damage degree quantitative index DF:

$$DF = \frac{k_{ij} - k_{jm}}{k_{0i}} \tag{18}$$

where k_{oi}, k_{ij}, k_{jm} are the slopes of the $0i$, ij, and jm segments, respectively.

With the continuous increase in the load, the slope of the load displacement gradually decreases with the formula satisfying $k_{oi} > k_{ij} > k_{jm}$. It can be found that when the position of the point m gradually moves to the destructive state, the variation of the slope of the ij and jm segments gradually decreases, showing that the damage degree of the corresponding position of the load–displacement curve increases as the quantization index decreases. It shows monotonicity of quantitative indicators and changes of actual damage degree, which proves that quantitative indicators meet physical meaning and change the trend of damage degree.

In this paper, the model arch static test was carried out by loading three-quarters of the points. The overall load displacement and the load–displacement curve of each measuring point position of 0# arch model are shown in Figs. **??** and **??**. It can be seen that the deflection trend of the arch is basically the same and can be regarded as a three-stage typical load–displacement curve. During the loading process, the deflection of different nodes is approximately antisymmetric, the deformation of 3L/4 loading point is obviously larger than the deformation of L/4 points and the deformation of vault is relatively small. When the breaking load is reached, the maximum deflection of 0# arch is 15.0 mm at the loading point, followed by that of quarter point section, which is 10.7 mm.

Since the final dynamic test shape of the model arch is a failure mode, the cracking point, the yield point and the failure point are taken as typical points of the load–displacement curve (as shown by the red line in Fig. **??**), and the damage degree of each test point of the model arch is respectively calculated according to the (18). The result is summarized in Table **??**, and the damage degree distribution is shown in Fig. **??**. The test is an eccentric load, the position of the near loading point is downward and the deflection of the far loading point is upward. This

Table 7
Summary of Damage Degree of 0 # Arch at Different Positions

	1	2	3	4	5	6	7
K_{01}	0.367	0.141	0.655	−1.2	−0.145	−0.093	−0.214
K_{12}	0.12	0.076	0.103	−0.593	−0.07	−0.047	−0.086
K_{23}	0.084	0.048	0.061	−0.216	−0.077	−0.038	−0.099
$(K_{12} - K_{23})/K_{01}$	0.099	0.196	0.065	0.314	−0.053	−0.784	−0.064

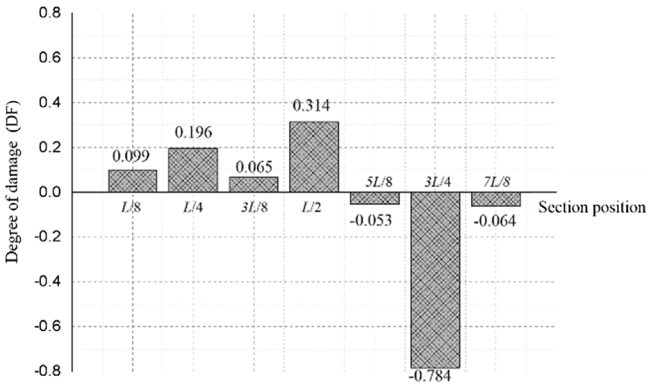

Figure 15. Damage distribution at different cross-sectional positions.

is because the direction of the bending moment at different positions is different under the action of the eccentric load, and the cracking position is different, so it is considered a positive value indicates a crack on the upper side of the arch section, and a negative value is a damage on the lower side. In addition, it can be clearly seen that except for the position of the vault, the damage degree of the other points is the same as the deflection of the same load. The damage degree is the highest at the 3L/4 position and the damage degree of the L/4 cross-section is the second. The results of the static test are the same; the damage of the loading point and the L/4 section are the most serious, indicating the feasibility of the dimensionless damage degree. Considering that the damage degree value at the position of the vault is far from the actual damage, it may be due to the small deflection of the vault position, the load–displacement curve is nearly parallel to the y-axis and the slope is close to infinity. Therefore, the damage of the vault position is not considered in the subsequent damage identification study.

4.3.2 Degree of Corrosion Damage

Through the accelerated corrosion test of arch 1# by electrochemical corrosion, the arch after electrochemical corrosion showed different damage states at different stages. Considering that the essential cause of corrosion damage of arch structure is internal steel corrosion producing corrosion products and corrosion expansion force; therefore, the actual corrosion rate of each section of reinforcement is taken as the indicator of corrosion damage degree in this paper.

4.4 Results of Damage Identification

4.4.1 Loading Damage Recognition

The degree of damage at different positions in Table **??** and the load damage index (the working condition II and the case I residual variance ratio) in Table **??** are plotted as the scatter plot for the x-axis and the y-axis, respectively, as shown in Fig. **??**. The scatter point is the corresponding position (*DF, DSF*) value, and the broken line is the line of fit for the correlation between the scatter points. Two conclusions can be adduced. (1) When the damage degree of RC arch is different, the damage index *DSF* of AR model and GARCH model shows a scattered distribution. The damage indexes under load damage are all less than 1, and the arch damage is aggravated with the increase in load, and the damage index is approximately linear change, which fully reflects the damage identification of RC arch based on the time series model under this index. (2) The data fitting of the damage index *DSF* and the damage degree *DF* can be found that the standard deviation of the fitting parameters (slope, intercept) of the AR model and the GARCH model is small, indicating that the parameters are reasonable. Compared with the AR model, the GARCH model is significantly better since the damage recognition accuracy of GARCH model is 89.1%, indicating that the GARCH model is more applicable to the RC arch loading damage identification. The correlation

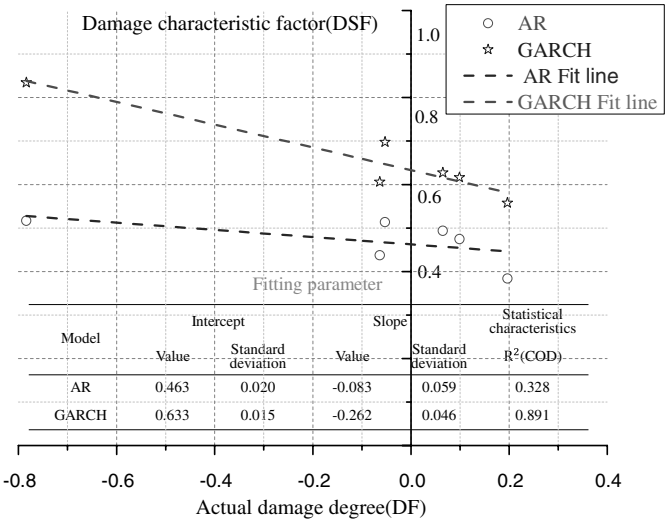

Figure 16. Loading damage identification.

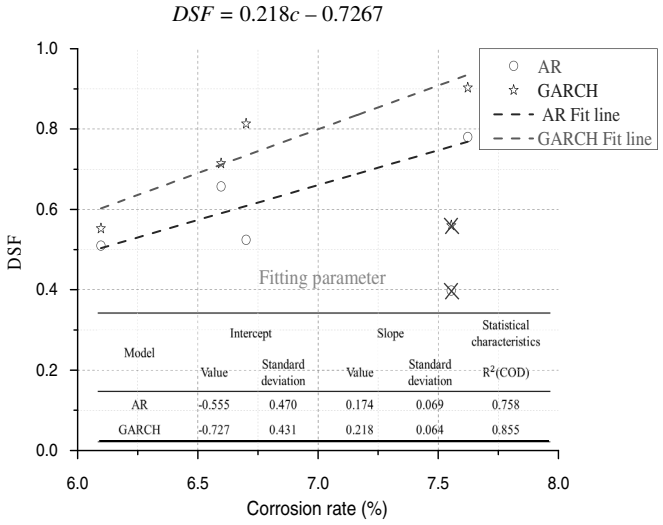

Figure 17. Corrosion damage identification.

between the damage index and the actual damage degree of the test arch reflects the recognition accuracy of different damage levels. Thus, based on the arch test data, it can be considered that the damage index *DSF* and the damage degree *DF* satisfy the following formula:

$$DSF = -0.262DF + 0.633 \tag{19}$$

4.4.2 Corrosion Damage Identification

As described in the previous section, the corrosion damage corresponding to the degree of damage (corrosion rate c) and the damage characteristic factor is made into scatter plots as in Fig. **??**, where the scatter points are the corresponding (c, DSF) values at different locations and the dashed lines are the correlation fitted curves between the scatter points. Three conclusions can be adduced. (1) The AR model and GARCH model damage identification deviations at the vault position are large and can be considered as error terms, so the coordinates of this position are treated as test deviation values and are not studied for correlation. (2) The damage characteristic factors differed significantly when the corrosion rates of different sections were different and increased gradually with the corrosion rate, indicating that the time series model can effectively identify the arch model damage caused by reinforcement corrosion. (3) A correlation study between the damage characterization factor DSF and the corrosion rate found that the standard deviation of the fitted parameters (slope, intercept) for both the AR and GARCH models were small, indicating significant parameter rationality. Moreover, the correlation between damage characteristic index and corrosion rate was better (75.8% for the AR model and 85.5% for the GARCH model), and in comparison, the fitted correlation of the GARCH model was slightly better than that of the AR model with an accuracy improvement of 12.8%. Therefore, it is considered more appropriate to use the following (20) for quantitative identification of corrosion damage:

$$DSF = 0.218c - 0.7267 \tag{20}$$

5. Conclusion

To accurately identify the damage state of arch bridges, a damage identification method combining Kalman filter, ARMA model and GARCH model for in-service arch bridges is proposed. The validity of this method is verified experimentally and some conclusions can be summarized as follows:

1. The intrinsic connection between structural vibration systems and time series models is derived. Experiments prove the validity of the proposed damage feature factors, which lay the foundation for the further application of the proposed method in the identification of arch bridge damage.
2. The linear time series ARMA model achieved 32.8% and 75.8% accuracy of model damage identification in loading damage state and corrosion damage state, which proved to be effective for simple structural damage identification. In response to the random errors associated with acceleration data in the linear time series model and the deficiency for heteroskedasticity, the combined Kalman–ARMA–GARCH structural damage identification method proposed in this paper achieves an accuracy of 89.1% and 85.5% for the model damage identification in the loading damage state and corrosion damage state, respectively, which verifies the effectiveness of the proposed method in damage identification.
3. From the comparison of the identification results of linear and nonlinear time series models, it is found that the feasibility of a linear time series model is low when the structure is damaged by loading. When the structure is corrosion damaged, the GARCH model identifies better than the AR model, and it improves the accuracy by 12.8%. The method also has theoretical advantages, which further proves the superiority of the arch bridge damage identification method based on the Kalman–ARMA–GARCH model.

The method proposed in this paper is used to identify the damage of the test arch under loading and corrosion, and good results are obtained, which proved the effectiveness and superiority of this method. However, in the case of coupled loading and corrosion damage, the method is worth further study.

Acknowledgement

The supports by Chinese Fundamental Research Funds for the Central Universities (SWU119051) and Basic Frontier Technology Research Topics of Chongqing (2017jcyjAX0229) are greatly acknowledged.

References

[1] P. Lu, D. Li, T. Hong, Y. Chen, and Q. Shi, Concrete performance time-varying effect of CFST arch bridges, *Mechanics of Time-Dependent Materials,* 2021, 1–19.

[2] H. Zhang, L. Liao, R. Zhao, J. Zhou, and M. Yang, The non-destructive test of steel corrosion in reinforced concrete bridges using a micro-magnetic sensor, *Sensors, 16*(9), 2016, 1439.

[3] W. Fan and P. Qiao, Vibration-based damage identification methods: A review and comparative study, *Structural Health Monitoring, 9*(1), 2011, 83–111.

[4] Y. Yan, L. Cheng, Z. Wu, and L. Yam, Development in vibration-based structural damage detection technique, *Mechanical Systems and Signal Processing, 21*(5), 2007, 2198–2211.
[5] I. Caliò, A. Greco, and D. D'Urso, Structural models for the evaluation of Eigen-properties in damaged spatial arches: A critical appraisal, *Archive of Applied Mechanics, 86*(11), 2016, 1–15.
[6] D. Capecchi, J. Ciambella, A. Pau, and F. Vestroni, Damage identification in a parabolic arch by means of natural frequencies, modal shapes and curvatures, *Meccanica, 51*, 2016, 2847–2859.
[7] S. Di, D. Zhang, and J. Li, Modal parameter identification of structure based on ITD method, *Journal of Civil Engineering and Management, 29*, 2012, 15–19.
[8] S. Jiang and C. Hu, Structural damage identification based on modal indices and data fusion for an arch bridge of concrete-filled steel tubes, *Journal of Vibration and Shock, 28*, 2009, 91–95, 204–205.
[9] Z. Nie and H. Ma, Structural damage detection based on reconstructed phase space, *Chinese Journal of Solid Mechanics, 34*, 2013, 83–92.
[10] L. Tan, *A Study on Reliability Method for Structural Damage Identification Based on Dynamic Fingerprints* (Guangzhou, Guangdong Province: South China University of Technology, 2010).
[11] Z. Wang and Y. Cheng, Structural damage identification based on sensitivity analysis of autoregressive coefficients of time series models, *Engineering Mechanics, 25*, 2008, 38–43, 49.
[12] M.Gul and F.N. Catbas, Structural health monitoring and damage assessment using a novel time series analysis methodology with sensor clustering, *Journal of Sound and Vibration, 330*, 2011, 1196–1210.
[13] Y.Du, W. Li, H. Li, and D. Liu, Structural damage identification based on time series analysis, *Journal of Vibration and Shock, 31*, 2012, 108–111.
[14] H.T. Pham and B.S. Yang, Estimation and forecasting of machine health condition using ARMA/GARCH model, *Mechanical Systems and Signal Processing, 24*(2), 2010, 546–558.
[15] L.J. Chen and L. Yu, Structural nonlinear damage identification algorithm based on time series ARMA/GARCH Model, *Advances in Structural Engineering, 16*(9), 2013, 1597–1609.
[16] C. Xiong, H. Lu, and J. Zhu. Operational modal analysis of bridge structures with data from GNSS/Accelerometer measurements. *Sensors, 17*(3) 2017, 436.
[17] Z. Chen, T.K.T. Tse, S.M. Liu, J. Zhou, and Y. Zeng, Application of a self-adaptive Kalman filter approach in alignment control for an extra long span rail transit cable-stayed bridge, *Structure and Infrastructure Engineering, 13*(9), 2017, 1186–1197.
[18] D.J. Xu, Z.M. Wu, and Y.L. Huang, A new adaptive Kalman filter with inaccurate noise statistics, *Circuits, Systems, and Signal Processing, 38*(9), 4380–4404, 2019.
[19] Y. Jiang and G. Huang, Short-term wind speed prediction: Hybrid of ensemble empirical mode decomposition, feature selection and error correction, *Energy Conversion and Management, 144*, 2017, 340–350.
[20] J.X. Yang, G.C. Sha, Y.X. Zhou, G.P. Wang, and B.R. Zheng, Statistical pattern recognition for structural health monitoring using ESN feature extraction method, *International Journal of Robotics and Automation, 33*(4), 2018, 569–576.
[21] R.F. Engle, Autoregressive conditional heteroscedasticity with estimates of the variance of United Kingdom inflation, *Econometrica: Journal of the Econometric Society, 50*(4), 1982, 987–1007.
[22] T. Bollerslev, Generalized autoregressive conditional heteroskedasticity, *Journal of Econometrics, 31*, 1986, 307–327.
[23] Y. Jiang, G. Huang, X. Peng, Y. Li, and Q. Yang, A novel wind speed prediction method: Hybrid of correlation-aided DWT, LSSVM and GARCH, *Journal of Wind Engineering and Industrial Aerodynamics, 174*, 2018, 28–38.

Biographies

Shuchang Zhou studies now as an undergraduate student at Southwest University, Chongqing, China. Her current research interest is signal processing and adaptive filtering. e-mail: zsc2473823148@163.com

Yan Jiang received his Ph.D. degree in Civil Engineering from Southwest Jiaotong University, China, in 2019. He is a fully lecturer of Southwest University. His research interests include bridge health monitoring, wind engineering and structural safety evaluation. e-mail: xnjtjiangyan@163.com

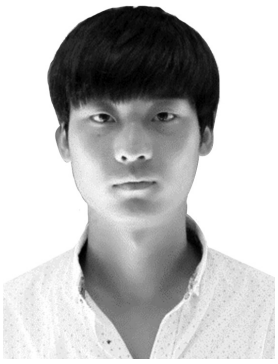

Xiaoqing Li received his master degree in Bridge and Tunnel Engineering in 2019. Now he is an engineer in China Design Group Co., Ltd. His current research interest is focused on structural design of long span bridge and structure safety evaluation.

Qingliang Wu received his Ph.D. degree in geotechnical engineering from University of Science and Technology Beijing in 2014. Now he is a lecturer in College of Engineering and Technology, Southwest University, China. His current research interests include safety monitoring and evaluation of geotechnical and structural engineering.